AJNR

3D Double-Echo Steady-State with Water Excitation MR Imaging of the Intraparotid Facial Nerve at 1.5T: A Pilot Study

Y. Qin, J. Zhang, P. Li and Y. Wang

AJNR Am J Neuroradiol 2011, 32 (7) 1167-1172
doi: https://doi.org/10.3174/ajnr.A2480
http://www.ajnr.org/content/32/7/1167

ORIGINAL RESEARCH

3D Double-Echo Steady-State with Water Excitation MR Imaging of the Intraparotid Facial Nerve at 1.5T: A Pilot Study

Y. Qin
J. Zhang
P. Li
Y. Wang

BACKGROUND AND PURPOSE: The intraparotid facial nerve is difficult to delineate using conventional MR sequence. Our aim was to assess the value of 3D DESSWE MR imaging in depicting the normal anatomy of the intraparotid facial nerve.

MATERIALS AND METHODS: A 3D-DESSWE sequence was performed with optimum parameters in 18 healthy volunteers on a 1.5T MR imaging unit. The data obtained were reconstructed in relation to the course of the facial nerve by using the MPR and thin-section MIP programs. Images acquired were analyzed by 2 neuroradiologists. They made the initial evaluations independently but resolved inconsistencies by collaborative review and consensus agreement. The certainty of identifying the intraparotid facial nerve was scored and recorded on an arbitrary scale of 0–2. The lengths of the facial nerves were measured; CNRs of the facial nerves and parotid ducts were calculated. Statistical evaluation of the results was achieved by the 2-tailed Wilcoxon test, ANOVA, and a paired *t* test.

RESULTS: In all subjects, 3D DESSWE images provided a reliable definition of the normal facial nerve anatomy bilaterally. There were no significant differences between scores, lengths, and CNRs of bilateral facial nerves ($P > .05$). The intraparotid facial nerve, parotid ducts, and retromandibular vein showed high signal intensity while the surrounding soft tissue showed relatively low signal intensity. The signal intensity between the facial nerves and parotid ducts was significantly different ($P < .01$); but no differences could be obtained for the CNRs between the 2 structures ($P > .05$).

CONCLUSIONS: The 3D DESSWE sequence can display the intraparotid course of the normal facial nerve, including the relationship between the facial nerve and the parotid duct.

ABBREVIATIONS: ANOVA = analysis of variance; BTFE = balanced turbo field echo; CNR = contrast-to-noise ratio; DESS = double-echo steady-state; DESSWE = double-echo steady-state with water excitation; FA = flip angle; FID = free induction decay; FISP = fast-imaging with steady-state precession; GRASS = gradient-recalled acquisition in the steady-state; MIP = maximum intensity projection; MPR = multiplanar reconstruction; PSIF = reversed fast imaging with steady-state free precession; SI = signal intensity; SNR = signal-intensity-to noise ratio; SSFP = steady-state free precession; WE = water excitation

Knowledge of the course of the facial nerve, which separates the deep and superficial lobes of the parotid gland, is helpful in determining the location of a parotid neoplasm. Various strongly T2- or T2*-weighted volume 3D fast MR imaging sequences have been advocated for evaluation of the cerebellopontine angle cistern and internal auditory canal segments of the facial nerve due to the natural contrast between the facial nerve and CSF.[1-3] However, visualization of the intraparotid facial nerve is limited with such sequences.[2]

T1-like volume 3D fast MR imaging sequences based on gradient-echo techniques, such as GRASS and magnetization-prepared rapid acquisition gradient echo, have been recommended to depict the intraparotid segments of the facial nerve.[4-6] In these imaging sequences, the intraparotid facial nerve and parotid ducts appear as low-signal-intensity lines surrounded by high-signal-intensity, especially fatty, parotid gland tissue. Recently, Tsang et al[7] compared BTFE with GRASS sequences at 1.5T and 3T. In their study, the facial nerve showed hypointensity on both sequences, while the parotid ducts showed hyper- and hypointensity on BTFE and GRASS sequences, respectively. This advantage facilitated differentiating the facial nerve from the parotid ducts.

However, there have been some contradictions in depicting the intraparotid facial nerve by using T1-like sequences. With the T1-weighted 3D fast low-angle shot (gradient-echo) sequence, which is similar to the GRASS sequence, Kraff et al[8] claimed that in general, they could not reproduce the results of former publications[4,6] at 7T. In their study with 4 subjects, the intraparotid facial nerve could only be presumably depicted close to the base of the skull; these findings are similar to those of a publication from Jäger and Reiser.[9]

A 3D-DESS sequence combined with a WE technique has been routinely used for orthopedic imaging to evaluate the articular cartilage.[10,11] To our knowledge, the present study is the first in which the intraparotid course of the facial nerve has been evaluated by using 3D-DESSWE images.

Received June 5, 2010; accepted after revision November 26.

From the Department of Radiology (Y.Q., P.L., Y.W.), First Affiliated Hospital, Tianjin University of Traditional Chinese Medicine, Tianjin, China; and Department of Radiology (Y.Q, J.Z.), Tianjin Medical University General Hospital, Tianjin, China.

This work was supported by Tianjin Municipal Nature Science Foundation (No. 09JCYBJC11500), the National Basic Research Program of China (973 program, No. 2010CB732506), and the National Natural Science Foundation of China (No. 30730036).

Please address correspondence to Jing Zhang, MD, Department of Radiology, Tianjin Medical University General Hospital, Tianjin 300052, China; e-mail: Zhangjingmd2002@hotmail.com

DOI 10.3174/ajnr.A2480

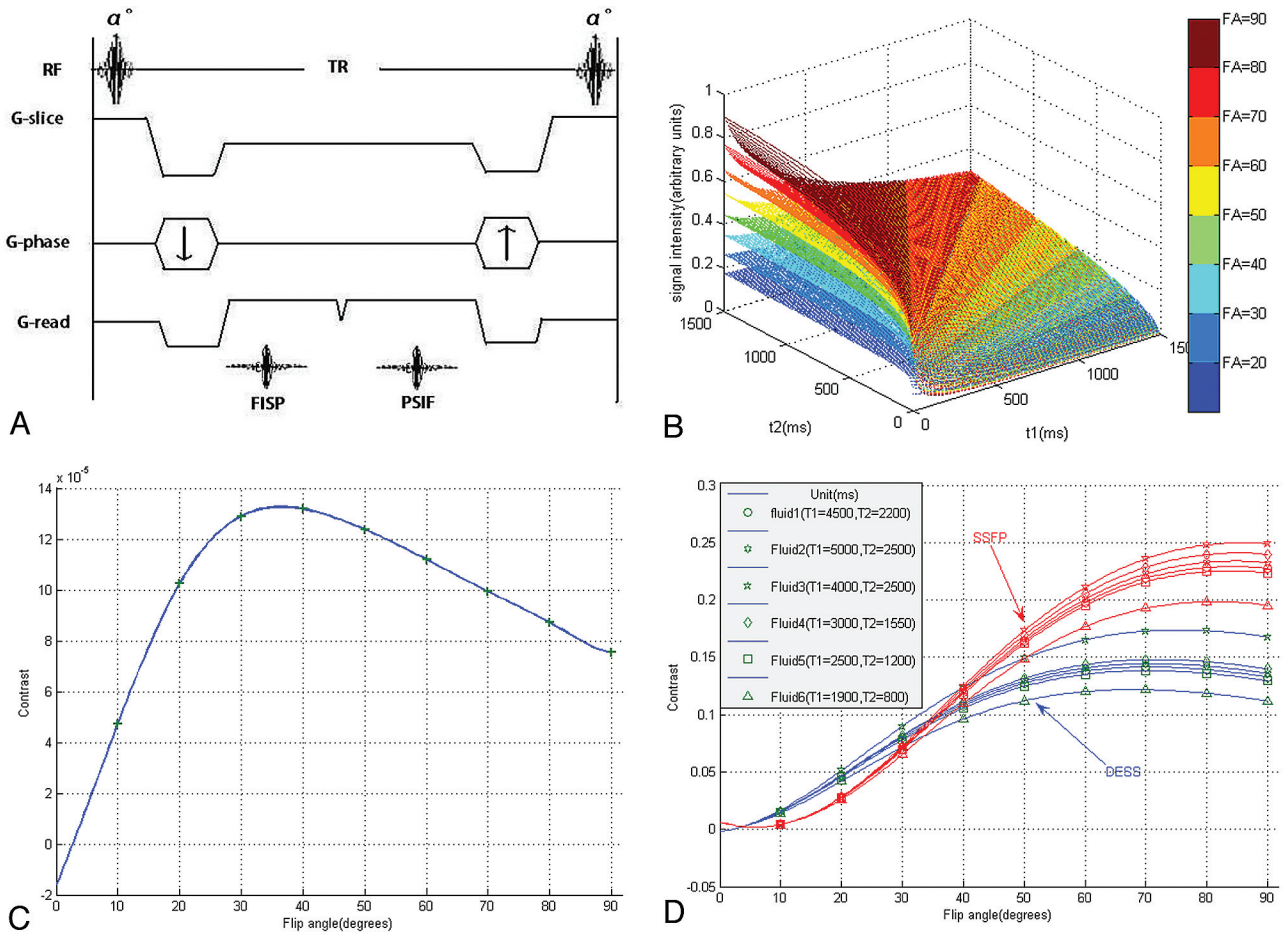

Fig 1. *A*, DESS sequence timing diagram. The DESS sequence samples 2 types of signals: One FID (FISP) echo is sampled immediately after each radio-frequency pulse, while the remaining transverse magnetization is refocused just before the next excitation pulse to form a spin-echo (PSIF) signal intensity. *B*, The signal intensity of the DESS sequence is simulated as a function of an FA from 20° to 90° for the assumed area (T1 = 0–1500 ms and T2 = 0–1500 ms, with an interval of 10 ms, 150 × 150 points). *C*, The factor of contrast between gray and white matter is simulated as a function of FAs from 10° to 90°. *D*, With the average of gray/white matter (T1 = 800 ms, T2 = 90 ms) as the reference substance, the factors of several fluid contrasts are simulated as a function of FAs from 10° to 90° for DESS (blue lines) and conventional SSFP (red lines) sequences.

Materials and Methods

Subjects

The study group included 18 volunteers (8 women and 10 men; mean age, 48.5 ± 9.8 years; range, 20–59 years) with no neurologic symptoms or neurologic diseases. Before beginning the study, all subjects gave written informed consent to participate in our departmental review board–approved protocol.

Optimization of Acquisition Parameters

The DESS sequence generates FISP and PSIF signals that are characterized with a different contrast behavior (Fig 1*A*). To optimize the image contrast, we first performed computer simulations of this sequence by using the equations through code written in Matlab 7.1 (MathWorks, Natick, Massachusetts). The relationship between signal intensity and acquisition parameters (TR, TE, FA, T1, T2) of the DESS sequence is shown in equations 1-3.[12,13] To remain in fast steady-state conditions and to shorten the total acquisition time, we set the TR and TE at 26 and 9 ms, which are the minimum values for the present sequence. Because most tissues are composed of numerous points with different parameters (T1, T2, and ρ) and the differences in proton attenuation are generally much smaller than the differences in relaxation times, to reduce the number of variables, we did not take the proton attenuation ρ into account in this simulation. For the overall evaluation, the T1 and T2 relaxation times of the parotid gland region were assumed to be within the range of 0–1500 ms and the FA degree was the only variable. In general, this simulation showed that the signal intensity of the DESS sequence enhanced as the FA increased (Fig 1*B*).

To the best of our knowledge, T1 and T2 values of normal parotid gland tissues and the facial nerve have not been reported. While the gray and white matter are considered as a reference for many radiologists to evaluate the contrast with different sequences, the contrast between 2 different tissues was computed from equation 3 provided by Dufour et al.[12] T1 and T2 values were taken as averages between gray and white matter at 1.5T with T1 = 800 ms, T2 = 90 ms, $\Delta T1$ = 10 ms, and $\Delta T1 / T1 = \Delta T2 / T2$.[12] Another optimization of FA was performed for the contrast between the fluid and parenchyma due to the former reports of nerve duct confusion.[4,6,7] To check the soundness of the simulation result, we computed a conventional SSFP sequence (equation 5), which had been in widespread use in our clinic, the same way.[14] All curves above were fitted by means of the nonlinear least squares method.

At FA = 40°, good gray/white matter contrast was acquired, whereas good contrast between the fluid and parenchyma was obtained at FA = 70° (Fig 1*C*, -*D*). Moreover, as a reference standard, the curve of conventional SSFP sequence coincided with the theoretic

derivations (Fig 1*D*), which had been verified by Wu et al.[15] To avoid system errors from the computation, we initially studied the first 3 volunteers with 3 FAs of 30°, 40°, and 50°. With FAs of both 40° and 50°, the facial nerve was well depicted. At FA = 50°, the signal intensity of the parotid ducts is a little higher than that at FA = 40°. To avoid the possible confusion between the intraparotid facial nerve and parotid duct, we then chose the present FA = 50°.

$$1)\qquad S_{FISP} = \frac{M_0 e^{-TE/T_2}\sin\alpha}{1+\cos\alpha}[1-(E_1-\cos\alpha)],$$

$$2)\qquad S_{PSIF} = \frac{M_0 e^{-TE/T_2}\sin\alpha}{E_2(1+\cos\alpha)}[1-(1-E_1\cos\alpha)D],$$

$$3)\qquad S_{DESS} = (S_{FISP} + S_{PSIF})/2,$$

$$4)\quad Contrast = S_{DESS}(T_1+\Delta T_1, T_2+\Delta T_2) - S_{DESS}(T_1-\Delta T_1, T_2-\Delta T_2),$$

where

$$5)\quad D = [(1-E_2^2)/(1-E_2^2E_1^2-2E_1\cos\alpha(1-E_2^2)+(E_1^2-E_2^2)\cos^2\alpha)]^{1/2},\ E_1 = e^{-TP/T1},\ E_2 = e^{-TR/T2},$$

$$S_{SSFP} = \frac{M_0\sin(\alpha)}{(1+T1/T2)+(1-T1/T2)\cos(\alpha)}\ (\text{with TR}\ll\text{T1 and TR}\ll\text{T2}).$$

where M_0 is the equilibrium magnetization.[15]

MR Imaging Procedures

Data were obtained on a 1.5T unit (Symphony; Siemens, Erlangen, Germany) by using a circularly polarized head array coil with 4 channels. After conventional T1- and T2-weighted spin-echo sequences, the 3D-DESSWE sequence was performed. Parameters were as follows: TR = 26,TE = 9.0 ms, FA = 50°, FOV = 200 × 200 mm (210 × 210 mm was used in 1 volunteer with a relatively large head), slab thickness = 96.0 mm, matrix = 512 × 192, number of 3D partitions = 64, number of slabs = 1, effective section thickness = 1.5 mm, number of acquisitions = 1, and scanning time = 10.41 minutes.

Image Analysis

The dataset from the 3D DESSWE sequence was reconstructed in 3 orthogonal oblique planes oriented in relation to the course of the facial nerve by using MPR and thin-section MIP functions. The distance of the cut for MPR was 0.4 mm, and the MIP thickness was dominated by the caliber of the structures studied. The images acquired were compared with anatomic diagrams in *Gray's Anatomy*[16] and analyzed by 2 experienced neuroradiologists. They made the initial evaluations independently but resolved inconsistencies by collaborative review and consensus agreement. The certainty of identifying the intraparotid facial nerve was scored and recorded on an arbitrary scale of 0–2 (homogeneity and facial nerve identified with certainty, 2; mild inhomogeneity and facial nerve probably identified, 1; severe inhomogeneity and facial nerve not identified, 0).[17-19] The length of the inpraparotid facial nerves, SI, and the corresponding SD of the nerves, parotid ducts, and parenchyma were measured by the 2 independent viewers. SNR = SI / SD of the 3 structures was first calculated. Then, CNR = $SNR_1 - SNR_2$ was calculated between the facial nerve (SNR_1) and the background parotid parenchyma (SNR_2); the parotid duct (SNR_1) was calculated the same way.

Table 1: Symmetry of the facial nerve[a]

	Right	Left	*P* value
CNR[a]	7.2 ± 3.5	8.2 ± 4.4	.483 ($t = -0.794$)
Length (mm)[b]	16.3 ± 4.9	15.4 ± 4.6	.227 ($t = 1.254$)
Score[c]	1.5 ± 0.42	1.55 ± 0.45	.564 ($z = -5.77$)

[a] Data are presented as mean ± SD.
[b] Paired *t* test.
[c] Wilcoxon test.

Table 2: Evaluation of facial nerves and parotid ducts[a]

	CNR	SNR	SI	SD
Facial nerve ($n = 36$)	7.7 ± 4.0	12.7 ± 4.2	91.2 ± 15.2	7.9 ± 2.5
Parotid duct ($n = 24$)	6.6 ± 3.4	11.5 ± 3.1	127.1 ± 51.2	11.6 ± 4.9
P value (ANOVA)[b]	.266 (1.261)	.258 (1.305)	0 (16.366)	0 (15.211)
P value (paired *t* test)[b]	.144 (1.514)	.144 (1.514)	0 (−4.232)	.001 (−3.882)

[a] Data are presented as mean ± SD.
[b] ANOVA and paired *t* test, with data in parentheses, are F and *t* values, respectively. Parotid ducts (24 bilateral), which could be identified, were tested with ipsilateral facial nerves.

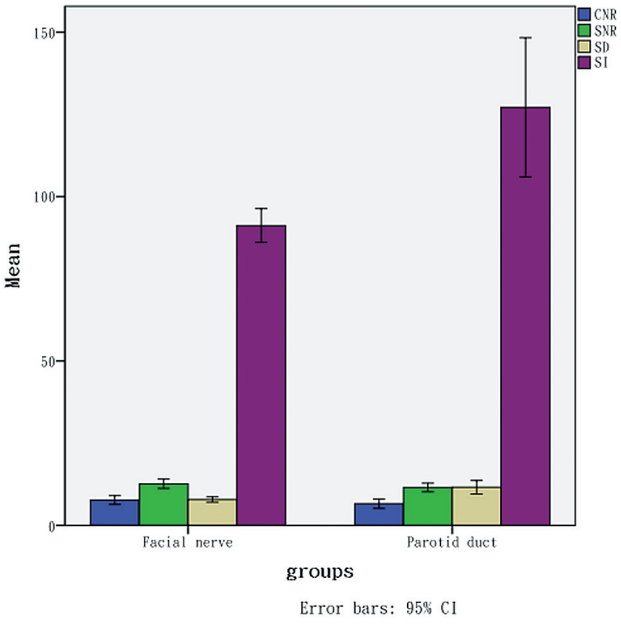

Fig 2. Note that both SI and SD of the parotid ducts are higher than those of the facial nerves, but there is no obvious difference between both structures for SNR and CNR.

Statistical Analysis

For overall analysis of the facial nerve, descriptive statistics for the qualitative data were developed after pooling right and left sides, whereas the quantitative data were averaged across both sides. This procedure was to simplify the presentation of results. Side-to-side symmetry of the independent qualitative assessments was evaluated on paired (left and right) data by using a Wilcoxon test. For the quantitative measurements, paired *t* testing was used to assess facial nerve side-to-side differences. Further comparison between the facial nerves and the ipsilateral parotid ducts was performed by using 1-way ANOVA and a paired *t* test. All tests for statistical significance were performed for 2-tailed hypotheses with $P < .05$. Statistical calculations were performed with the Statistical Package for the Social Sciences, Version 18 (SPSS, Chicago, Illinois).

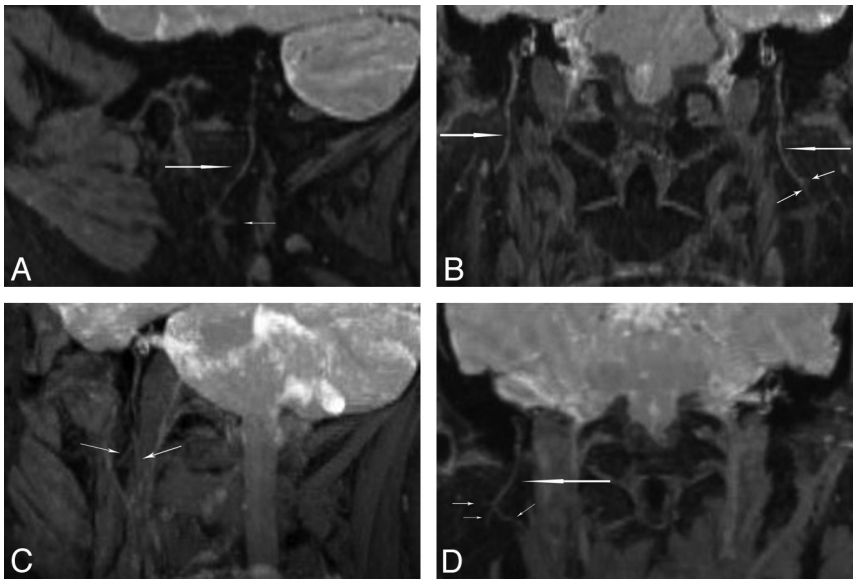

Fig 3. Oblique-sagittal coronal MPR (*A* and *B*) and MIP (*C* and *D*) images of the intraparotid facial nerve demonstrate its cervicofacial division (*long arrows*) and small branches (*short arrows*). The cervicofacial division separates the deep and superficial lobes of the parotid gland.

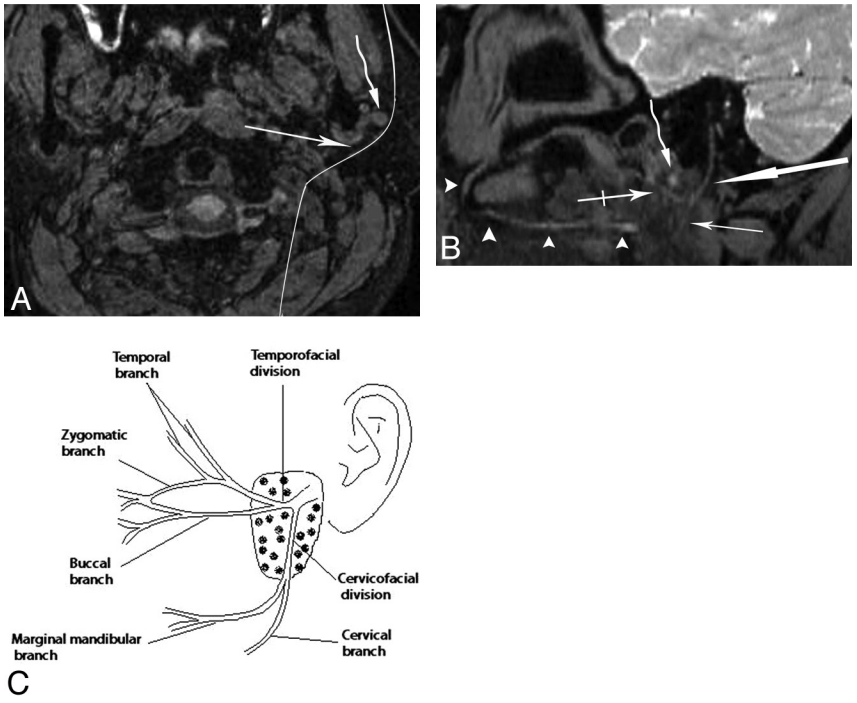

Fig 4. *A,* The axial source image shows a curved reconstruction plane (*long curved line*), which is behind the retromandibular vein, following the main course of the facial nerve and parotid duct. *B,* The curved MPR reconstructed image shows the main trunk of the facial nerve (*thick arrow*) and the bifurcation of the temporofacial (*crossed arrow*) and the cervicofacial (*thin arrow*) divisions, which is posterior and inferior to the retromandibular vein (*curved arrow*). The course of the parotid duct (*arrowheads*) from the hilus of the gland to the mouth is shown. *C,* Diagram illustrates 1 pattern of the intraparotid facial nerve branching.

Results

All 3D DESSWE MR images were successfully obtained on 18 healthy volunteers. The normal facial nerve showed high signal intensity, while the soft tissue surrounding it showed relatively low signal intensity. The main trunks and cervicofacial divisions of the facial nerve were identified (score 2 or 1) in 100% (36/36) and 94.4% (34/36), respectively; the temporofacial divisions of the nerve were identified (score 2 or 1) in 55.6% (20/36). No statistical difference was obtained for both sides of the facial nerve ($P > .05$) (Table 1).

The parotid ducts were identified in 66.7% (24/36) and showed high signal intensity in the anteroinferior segment of the parotid gland. The parotid ducts, which could be identified (24 pairs), were analyzed statistically by using ANOVA and a *t* test for paired data with the same side of the facial nerves. For SI and SD, there were significant differences be-

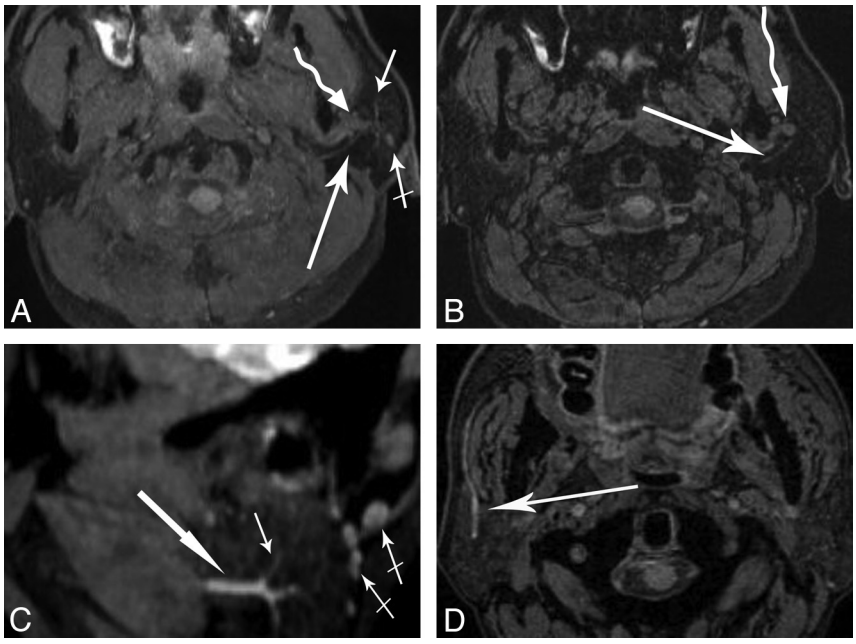

Fig 5. *A* and *B*, Axial MIP image (*A*) and source image (*B*) show the facial nerve (*long arrow*) and retromandibular vein (*curved arrow*). In the MIP image, more information concerning the branches of the parotid duct (*short arrow*) and lymph node (*crossed arrow*) is demonstrated, and the length of the facial nerve is shown to be longer than that in the source image. *C* and *D*, Sagittal MIP image (*C*) and axial source image (*D*) show that the parotid duct (*long arrows*) is in the anterior and inferior portion of the gland. In the sagittal MIP image, the branches of the parotid duct (*short arrow*) and lymph nodes (*crossed arrow*) are shown.

tween the nerves and ducts ($P < .01$), but no differences were obtained from CNRs and SNRs ($P > .05$) (Table 2 and Fig 2). The retromandibular vein, which showed high signal intensity in axial source images, was identified in 66.7% (24/36).

Oblique-sagittal and coronal reconstructed images demonstrated the main trunks and cervicofacial divisions (Fig 3). Curved reconstructed images could display the bifurcation of the temporofacial and cervicofacial divisions with the parotid ducts in 1 image (Fig 4*A*, -*B*). Oblique axial reconstructed images showed the main trunk and initial part of the temporofacial nerve (Fig 5*A*); sagittal reconstructed images showed the parotid duct (Fig 5*C*). The reconstructed images presented more information than the source images (Fig 5*B*, -*D*).

Discussion

The DESS sequence involves the acquisition of 2 different echoes during each TR based on the SSFP technique. The first echo is the FID gradient echo used in the FISP sequence, and the second is the radio-frequency echo (spin-echo) used in the PSIF sequence. PSIF signal intensity accentuates the signal intensity of the components with long T2s, such as CSF; FISP signal intensity provides more anatomic details with a contrast dominated by the T1/T2 ratio.[12-14,20] The WE technique has been recommended in combination with SSFP-type sequences for orthopedic and cine cardiovascular imaging.[10,11,21] With this technique, only water is excited by using section-selective composite pulses, while lipid spins are left in equilibrium, providing advantages of no disruption of the steady-state and uniform fat suppression.

Visualization of the intraparotid facial nerve on T1-like images depends on the content of the fatty tissue.[4,6] The use of fat saturation will make the fat disappear and blur the margin between the nerve and surrounding soft tissues. However, the fat saturation, namely the WE technique combined with the DESS sequence, allows the facial nerve itself to be clearly shown without relying on the fatty tissue background, which is different from studies heretofore.[4-8] However, features of images of this sequence are similar to those of images from the 3D PSIF with diffusion-weighted MR imaging, which is newly presented by Zhang et al,[22] specifically designed for cranial nerve imaging on their 3T MR imaging unit. DESS sequences include both FISP (FISP is a synonym for GRASS) and PSIF sequences, which have been reported as alternatives to depict the extracranial facial nerve.[4,6,22]

The DESSWE sequence involves flow sensitivity, because the intensity of the moving spins depends on the ability to reach a new steady-state in a limited period of time.[12] The stationary fluid (venous blood and saliva in parotid ducts) showed high signal intensity, whereas the moving fluid (blood in the external carotid artery) revealed a signal-intensity void. This feature proved to be an advantage of displaying the facial nerve near the vessels with fast-flow velocity in the parotid gland. Sometimes, if it could be identified, the retromandibular vein in axial source images could be used as a landmark to seek temporofacial and cervicofacial divisions because, in most cases, the intraparotid facial nerve branches into the 2 main trunks just behind it.

Because of the high noise (SD) of the parotid ducts, no statistical differences of the CNRs were obtained between the nerves and ducts (Fig 2). From our point of view, in the present study, this situation mainly resulted from the following causes: 1) Although the oversampling for this sequence increased to 100%, the wrap artifacts from the upper portion of the head (frequency selection direction) could not be eliminated if the parotid ducts were not at the lower border of the FOV (Fig 5*A*). 2) For the parotid ducts, the optimum FA selected by computation was 70°, but it was not a selected struc-

ture in this study. 3)The susceptibility artifacts from the oral cavity disturbed the parotid duct more seriously than the facial nerve due to its closer range. Nevertheless, the signal-intensity difference between both structures was conducive to differentiating the facial nerves from the parotid ducts in the present study. However, confirming the facial nerve still requires combining its pathway and position.

The oblique axial reformatted images with planes angled caudal and cephalad to the orbital-meatal line were routinely used to depict the cervicofacial and the temporofacial divisions of the intraparotid facial nerve.[6,7,23] In our study, the axial images were the source dataset of the 3D-DESSWE sequence, due to its character of steady-state for flowing spins in the retromandibular vein and the external carotid artery, which are perpendicular to the axial sections.[12] However, our results showed that the oblique sagittal and coronal planes, which were reconstructed following the main trunk of the intraparotid facial nerve, appear to be the more appropriate planes for evaluating the cervicofacial division (Fig 3).

Compared with the cervicofacial division (identified in 94.4%), the temporofacial division was more difficult to represent (identified in 55.6%) in the present study because it diverges from the main trunk at a sharp angle. The method of curved sagittal reconstructions proposed by Dailiana et al[4] could delineate the intraparotid facial nerve (main trunk and the cervicofacial and the temporofacial divisions of the facial nerve) and the parotid duct in 1 image (Fig 4*A*, -*B*). The initial part of it could be defined by following the main trunk with the selected angled axial images (Fig 5*A*, -*B*).

The 3D-DESSWE MR imaging in the present study has several advantages over conventional MR imaging. First, this sequence has higher SNR because 2 echoes were sampled during each TR. Second, the WE technique improved contrast enhancement by saturating the background soft tissue. Third, the signal intensity of the 3D-DESSWE sequence, with features of an SSFP technique, strongly depends on the steady-state condition. This feature will contribute to defining the bifurcation of the intraparotid facial nerve by the retromandibular vein, distinguishing the nerve from the parotid ducts, and depicting the nerve sections located near the external carotid artery.

Besides susceptibility and motion artifacts on the DESSWE images, there are several limitations in present study. First, the aimed structure of the facial nerve was not in the center of the FOV, and the parotid duct was at the lower border of it, to avoid the wrap artifacts. This degraded the image quality in the facial nerves, especially the parotid ducts. Second, compared with other conventional fast sequences, the scanning time of the sequence is slightly prolonged due to the acquisition of 2 different echoes during each TR. Third, because of the combination of FISP-like and strong T2 contrast (PSIF), the use of this sequence may increase the complexity in terms of analyzing the pathologies within the parotid gland. Finally, a surface coil, which was reported as contributing to identifying the intraparotid nerve, was used in this study.[5-7]

Conclusions

The 3D-DESS sequence is an SSFP-type gradient sequence with unique contrast and high SNR. When combined with the WE technique, this sequence can display the intraparotid course of the normal facial nerve. Further refinement of the 3D-DESSWE sequence will require a surface coil. A high-field MR imaging unit may reduce the scanning time and keep the high SNR feature. This approach may also contribute to depicting the extracranial part of other cranial nerves.

Acknowledgments

We thank Li jin-ting, MD, for helpful discussions.

References

1. Shinji N, Tokiko K, Hiroshi F, et al. **MR cisternography of the cerebellopontine angle: comparison of three-dimensional fast asymmetrical spin-echo and three-dimensional constructive interference in the steady-state sequences.** *AJNR Am J Neuroradiol* 2001;22:1179–85
2. Lane JI, Ward H, Witte RJ, et al. **3-T imaging of the cochlear nerve and labyrinth in cochlear-implant candidates: 3D fast recovery fast spin-echo versus 3D constructive interference in the steady state techniques.** *AJNR Am J Neuroradiol* 2004;25:618–22
3. Byun JS, Kim HJ, Yim YJ, et al. **MR imaging of the internal auditory canal and inner ear at 3T: comparison between 3D driven equilibrium and 3D balanced fast field echo sequences.** *Korean J Radiol* 2008;9:212–18
4. Dailiana T, Chakeres D, Schmalbrock P, et al. **High-resolution MR of the intraparotid facial nerve and parotid duct.** *AJNR Am J Neuroradiol* 1997; 18:165–72
5. Held P, Fellner C, Fellner F, et al. **MRI of inner ear anatomy using 3D MP-RAGE and 3D CISS sequences.** *Br J Radiol* 1997;70:465–72
6. Takahashi N, Okamoto K, Ohkubo M, et al. **High-resolution magnetic resonance of the extracranial facial nerve and parotid duct: demonstration of the branches of the intraparotid facial nerve and its relation to parotid tumours by MRI with a surface coil.** *Clin Radiol* 2005;60:349–54
7. Tsang JC, Yip WH, Lau CS, et al. **Visualization of normal intra-parotid facial nerve on MR: BTFE or GRASS?** *Clin Radiol* 2009;64:1115–18
8. Kraff O, Theysohn JM, Maderwald S, et al. **High-resolution MRI of the human parotid gland and duct at 7 Tesla.** *Invest Radiol* 2009;44:518–24
9. Jäger L, Reiser M. **CT and MR imaging of the normal and pathologic conditions of the facial nerve.** *Eur J Radiol* 2001;40:133–46
10. Knuesel PR, Pfirrmann CW, Noetzli HP, et al. **MR arthrography of the hip: diagnostic performance of a dedicated water-excitation 3D double-echo steady-state sequence to detect cartilage lesions.** *AJR Am J Roentgenol* 2004; 183:1729–35
11. Eckstein F, Hudelmaier M, Wirth W, et al. **Double echo steady state magnetic resonance imaging of knee articular cartilage at 3 Tesla: a pilot study for the Osteoarthritis Initiative.** *Ann Rheum Dis* 2006;65:433–41. Epub 2005 Aug 26
12. Dufour I, Bittoun J, Idy-Peretti I, et al. **Implementation and optimization by the simplex method of a 3D double echo sequence in steady-state free precession.** *Magn Reson Imaging* 1993;11:87–93
13. Hardy PA, Recht MP, Piraino D, et al. **Optimization of a dual echo in the steady state (DESS) free precession sequence for imaging cartilage.** *J Magn Reson Imaging* 1996;6:329–35
14. Bruder H, Fischer H, Graumann R, et al. **A new steady-state imaging sequence for simultaneous acquisition of two MR images with clearly different contrasts.** *Magn Reson Med* 1988;7:35–42
15. Wu ML, Ko CW, Chen TY, et al. **MR ventriculocisternography by using 3D balanced steady-state free precession imaging: technical note.** *AJNR Am J Neuroradiol* 2005;26:1170–73
16. Standring S. **Face and scalp.** In: Standring S, ed. *Gray's Anatomy: The Anatomical Basis of Clinical Practice.* 39th ed. London: Churchill Livingstone; 2004;497–517
17. Yousry I, Moriggl B, Schmid UD, et al. **Trigeminal ganglion and its divisions: detailed anatomic MR imaging with contrast-enhanced 3D constructive interference in the steady state sequences.** *AJNR Am J Neuroradiol* 2005;26: 1128–35
18. Linn J, Moriggl B, Schwarz F, et al. **Cisternal segments of the glossopharyngeal, vagus, and accessory nerves: detailed magnetic resonance imaging-demonstrated anatomy and neurovascular relationships**. *J Neurosurg* 2009; 110:1026–41
19. Linn J, Peters F, Moriggl B, et al. **The jugular foramen: imaging strategy and detailed anatomy at 3T.** *AJNR Am J Neuroradiol* 2009;30:34–41
20. Redpath TW, Jones RA. **FADE: a new fast imaging sequence.** *Magn Reson Med* 1988;6:224–34
21. Lin HY, Raman SV, Chung YC, et al. **Rapid phase-modulated water excitation steady-state free precession for fat suppressed cine cardiovascular MR.** *J Cardiovasc Magn Reson* 200810:22
22. Zhang Z, Meng Q, Chen Y, et al. **3-T imaging of the cranial nerves using three-dimensional reversed FISP with diffusion-weighted MR sequence.** *J Magn Reson Imaging* 2008;27:454–58
23. Teresi LM, Kolin E, Lufkin RB, et al. **MR imaging of the intraparotid facial nerve: normal anatomy and pathology**. *AJR Am J Roentgenol* 1987;148:995–1000